Investigating the Dynamics of Pt/CeO2 Catalysts at the Powder Agglomerate Scale by Combining In Situ Hyperspectral Raman Imaging and SEM-EDX Analysis

C. Molinet-Chinaglia, L. Piccolo, S. Loridant

Investigating the Dynamics of Pt/CeO_2 Catalysts at the Powder Agglomerate Scale by combining in situ hyperspectral Raman imaging and SEM-EDX analysis

Clément Molinet-Chinaglia,[a] Laurent Piccolo,[a] and Stéphane Loridant*[a]

[a] Dr. C. Molinet-Chinaglia, Dr. L. Piccolo, Dr S. Loridant

Univ Lyon, Université Claude Bernard-Lyon 1, CNRS, IRCELYON

2 av. A. Einstein F-69626 Villeurbanne Cedex (France)

E-mail: stephane.loridant@ircelyon.univ-lyon1.fr,

URL : https://www.ircelyon.univ-lyon1.fr/en/syrcel-en/card/SLO/

Supporting information for this article is given via a link at the end of the document.

Abstract: The dynamics of Pt/CeO_2 catalysts is a hot topic since its knowledge can be used to (re)generate more active sites for redox reactions, even at low temperature (<500 °C). While numerous works focus on the atomic scale, the spatial extent of Pt surface diffusion is poorly known. In this work, it is evaluated at the powder agglomerate scale using an original methodology combining SEM-EDX analysis and in situ optical/microRaman hyperspectral imaging performed on a Pt/CeO_2+CeO_2 mechanical mixture. No intergranular diffusion of platinum during redox cycles at 500 °C is revealed by these techniques, in particular by the Raman images of Ce^{3+} and peroxo species, which are highly sensitive to the presence of Pt atoms. It strongly suggests that Pt surface diffusion takes place only at the nanometer scale and could be limited by atom trapping on Pt/CeO_2 agglomerates. Our method for investigating diffusion processes at the micrometer scale may be extended to other thermochemical conditions and other materials.

Introduction

Pt/CeO_2 catalysts are widely used in many redox reactions such as the oxidations of CO and hydrocarbons for automotive exhaust depollution,[1] the water-gas shift reaction[2] and the preferential CO oxidation for pure H_2 production.[3] The Pt/CeO_2 system combines the unique redox properties of ceria,[4] the ability of oxygen vacancies to split water,[5] and that of platinum particles to chemisorb CO and dissociate H_2.

In spite of the abundant literature on the Pt/CeO_2 system, the debate on the nature of active Pt species (Pt nuclearity and oxidation state) for e.g. CO oxidation is still lively.[1,6-9] In fact, the Pt/CeO_2 catalytic performance is related to the geometric and electronic properties of Pt active sites and the metal-oxide interfacial structure,[10,11] which in turn depend on the reaction conditions.[12,13]

Pt single atoms (SAs) are prone to agglomerate into Pt clusters/nanoparticles under reducing atmosphere, while the strong Pt-O-Ce interaction favours redispersion of platinum as PtO_x clusters or SAs[13-16] such as Pt SAs trapped on ceria defects.[17,18] A square-planar arrangement of four oxygen atoms has been identified as an important structure to stabilize Pt^{2+} SAs.[19] Moreover, a restructuration of ceria has been evidenced by the formation of four-fold hollow sites for single atoms during oxidative treatment above 600 °C.[20]

Redispersion of Pt under oxidizing atmosphere via PtO_2 sublimation followed by atom trapping was shown to occur above 550 °C.[17, 21-23] However, vaporisation of PtO_2 is limited and slow at 550 °C.[24] Furthermore, Kwak et al. demonstrated that the diffusion of platinum and other transition metals could not be neglected inside the grain boundaries of ceria-based materials at 650 °C under reducing conditions.[25]

Rapid and efficient oxidative redispersion of large Pt agglomerates on a ceria-based oxide support during rapid redox cycling (60 s) was evidenced from X-ray absorption spectroscopy analysis at 500 °C and above, but not at 400 °C.[16] However, a high mobility and redispersion of Pt particles was observed already at 400 °C after 10 min under O_2 (2.5 mbar), especially for small nanoparticles (<2 nm), by Transmission Electron Microscopy (TEM) and Scanning Transmission Electron Microscopy (STEM).[26] Furthermore, the possibility to tune the Pt/CeO_2 catalytic properties from redox treatments at temperatures below 500 °C by controlling the size and morphology of Pt nanoparticles was highlighted.[12,26] Finally, redispersion of Pt deposited on CeO_2(111) was observed by Scanning Tunnelling Microscopy (STM) after 10 min exposure to 1×10^{-5} Pa O_2 at 27 °C, followed by flash annealing at 327 °C.[27]

Even if these advances were facilitated by in situ/operando spectroscopic and microscopic techniques providing characterization of Pt species under controlled atmospheres or reaction conditions,[28-31] the mechanism driving redispersion below 500 °C (without PtO_2 vaporization) is poorly discussed in the literature. It was however assumed a mass transport of Pt on CeO_2(111) surfaces via diffusion of Pt adatoms, the activation energy for Pt adatom hopping on clean CeO_2(111) calculated by Density Functional Theory (DFT) being 0.5 eV. It renders surface diffusion of Pt adatoms a fast and efficient process.[27]

However, numerous questions remain to be addressed, especially on the length scale of this surface diffusion phenomena, which could range from the crystallite scale (a few nanometers) to the powder agglomerate scale (a few tenths of microns).

In this context, the objective of this work was to determine whether the surface diffusion of Pt evidenced at the ceria crystallite scale also takes place at the powder agglomerate scale. At this scale, Pt is heterogeneously distributed in aged catalysts[32] and efficient regeneration needs redispersion over micrometric distances. A working temperature of 500 °C was chosen because it is high enough to favour surface diffusion of Pt atoms but low enough to avoid CeO_2 sintering and PtO_2 sublimation. To reach that purpose, an original method combining ex situ EDX analysis and in situ optical/microRaman hyperspectral imaging was implemented on a mechanical mixture of Pt/CeO_2 catalyst and bare CeO_2.

Results and Discussion

Characterization of the Pt/CeO2 Catalyst

The composition of the prepared Pt/CeO_2 catalyst determined by ICP was 0.80 wt%. It is labelled 0.80Pt in the following. Its XRD diffractogram provided in Figure S1 contains only the peaks of cubic CeO_2, suggesting that Pt was highly dispersed either as single atoms and/or clusters (size < 2 nm). The d crystallite size of CeO_2 obtained from Rietveld refinement is 6.4 ± 0.1 nm. Considering spherical particles and a ρ volume weight of 7.22 $g.cm^{-3}$ a specific surface area of $6/\rho d$=128 $m^2.g^{-1}$ was calculated, which is close to the BET value (150 $m^2.g^{-1}$). It reveals that the external surface of crystallites mostly contributes to the specific surface area. Furthermore, only CeO_2 crystallites were observed by STEM (Figure S2).

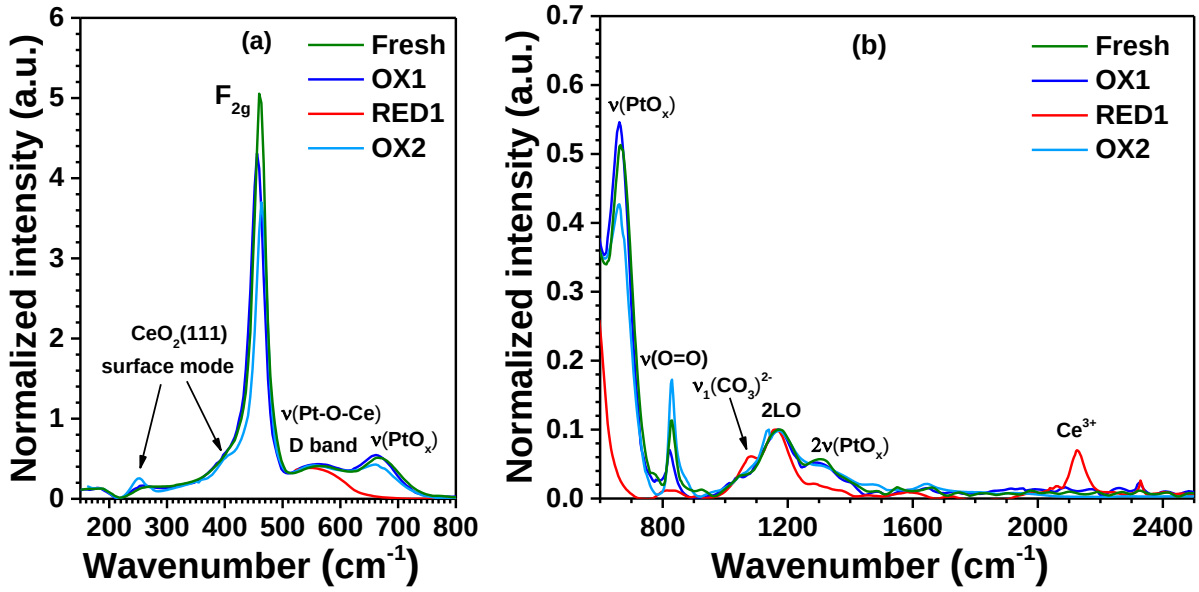

Figure 1. Raman spectra of 0.80Pt sample after OX1, RED1 and OX2 treatments (a) between 100 and 800 cm^{-1}, (b) between 600 and 2500 cm^{-1}. The spectra are presented after baseline subtraction and normalization on the 2LO band.

Raman spectra were recorded to determine the structure of the 0.80Pt catalyst during redox cycles (Figure 1). The main band at 464 cm^{-1} arises from the F_{2g} vibrational mode of cubic CeO_2, while the broad band around 1170 cm^{-1} corresponds to the second order 2LO mode.[33] The less intense features at 264, 402 cm^{-1} and at 550-600 cm^{-1} are respectively attributed to surface modes of clean CeO_2(111) crystalline plane and to the LO mode, which is activated by the presence of defects (including oxygen vacancies).[33] Furthermore, the bands at 560 and 650 cm^{-1} in the fresh state and after OX1 treatment are attributed to either ν_{as}(Pt-O-Ce) and ν_s(Pt-O-Ce) stretching vibrations[33,34] or ν(Pt-O-Ce) and ν(Pt-O) stretching vibrations[35] of PtO_x species highly dispersed on the surface of CeO_2. Note that the former band is superimposed to the defects band, also called D band. Finally, the thin band at 826 cm^{-1} is typical of ν(O=O) stretching vibrations of peroxo species adsorbed on oxygen vacancies.

The PtOx bands disappeared upon RED1 treatment, suggesting reduction of PtOx to Pt0 species.[12,33] Furthermore, the appearance of the band at 2130 cm^{-1} due to electronic Raman scattering of Ce^{3+} ($^2F_{5/2} \rightarrow {}^2F_{7/2}$ transition) reveals the presence of such cations.[33] Their formation originates from H_2 dissociation on Pt^0 species and subsequent hydrogen spillover on the CeO_2 surface, leading to formation of H_2O and replacement of O^{2-} anions by vacancies. Note that the ν(O=O) band is not observed at this step.

After reoxidation treatment (OX2), the $\nu(PtO_x)$ band reappears in the spectrum of 0.80Pt while the Ce^{3+} band disappears, showing reoxidation of the ceria support and the Pt^0 species. Note that the $\nu(PtO_x)$ band is slightly weaker after OX2 treatment while the ν(O=O) band is stronger, similarly to the spectral evolutions reported by Ferré et al. after such redox cycles.[12]

Note that even if Raman spectroscopy can be considered as a bulk technique with a probed depth of typically 1 μm, PtO_x species are located on the (sub)surface of crystallites and only the surface (few layers) of CeO_2 is reduced upon thermal treatment under H_2 at 500 °C.[36,37] Therefore, Ce^{3+} cations, oxygen vacancies and peroxo species formed by reaction with gaseous O_2 are mostly located on the surface and the Raman bands attributed to those species provide characterization of the surface.

Study of 0.80Pt+CeO_2 (1/1) Mechanical Mixture

In order to characterize the intergranular diffusion, mechanical mixtures of the 0.80Pt catalyst and the CeO_2 support were prepared to follow their potential homogenization during redox cycles at 500 °C. After various tests at different concentrations, a mixture with a 1/1 mass ratio was selected.

Optical images recorded using the Raman microscope after OX1 oxidative treatment show orange and yellow areas (Figure 2a) corresponding to agglomerates of 0.80Pt and CeO_2, respectively.

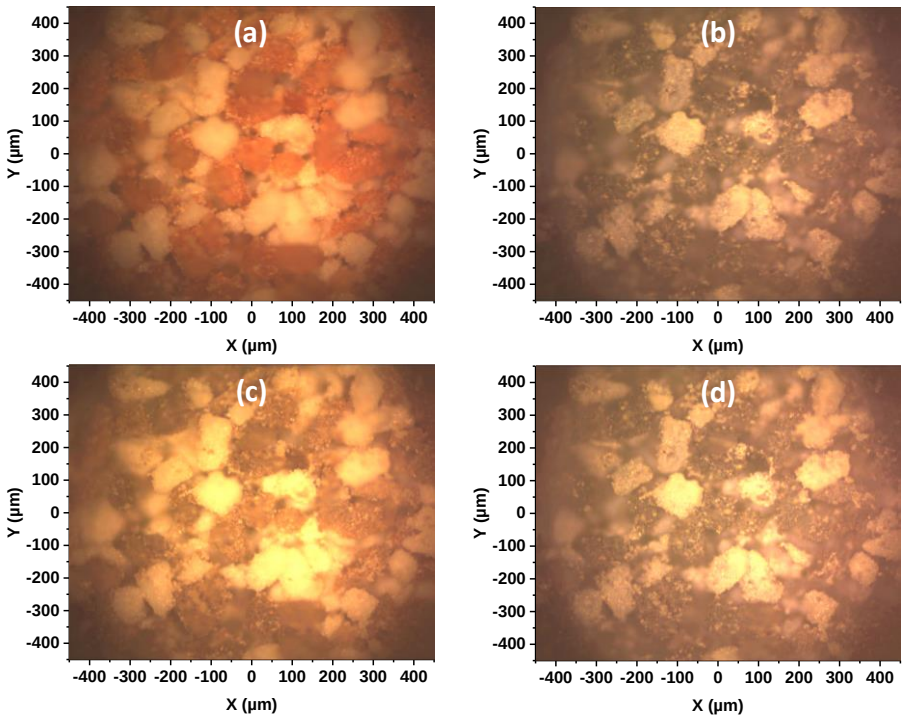

Figure 2. Optical images of 0.80Pt+CeO_2 (1/1) mechanical mixture recorded using a x50 objective at RT after (a) OX1, (b) RED1, (c) OX2 and (d) RED2 treatments.

The yellow colour comes from the presence of defects (oxygen vacancies, coloured centres) within the crystallographic lattice of nanocrystalline CeO_2.[38-40] On the other hand, the agglomerates of the 0.80Pt catalyst are orange, which results from the decrease in the band gap of ceria due to its interaction with platinum cations.[41] After reduction RED1 (Figure 1b), these agglomerates turned black due to the formation of Ce^{3+} absorbing strongly in the visible.[41] After reoxidation OX2 (Figure 1c), the colour of CeO_2 agglomerates was recovered while that of 0.80Pt became grey. Finally, the image of the mixture after the second reduction (RED2) is quite similar to that after RED1 treatment. These results suggest that platinum diffusion does not take place between the 0.80Pt catalyst and CeO_2 agglomerates. One hundred spectra of the fresh and pelleted mechanical mixtures were recorded over different areas by EDX analysis in the SEM apparatus. As expected, areas rich in platinum at about 0.80 wt% (Figure S3a) and areas poor in platinum at about 0 wt% (Figure S3b) were observed at the surface of the mechanical mixture. A statistical analysis reveals a bimodal distribution of the Pt amount (Figure 3), validating the choice of the granulometry and the mixture composition to follow the possible Pt diffusion during redox treatments. After the OX1/RED1/OX2 treatments of 1 h each, both populations are still observed (Figure 2), revealing no homogenization of the Pt content at the ceria agglomerate scale. This is confirmed for longer redox treatments (OX1/RED1/OX2, 10 h each, Fig. 2). The absence of homogenisation even after 10 hours could be related to loose contacts between agglomerates but note that this time is much longer than the 10 minutes enough to observe Pt redispersion on Pt/CeO_2

powder at only 400 °C. [26] It suggests a thermodynamics limitation of Pt surface diffusion on Pt/CeO_2 agglomerates or a high activation energy strongly slowing down its kinetics. However, surface diffusion of Pt on CeO_2(111) surfaces was reported as a fast and efficient process.[27] Therefore, the first assumption was preferred.

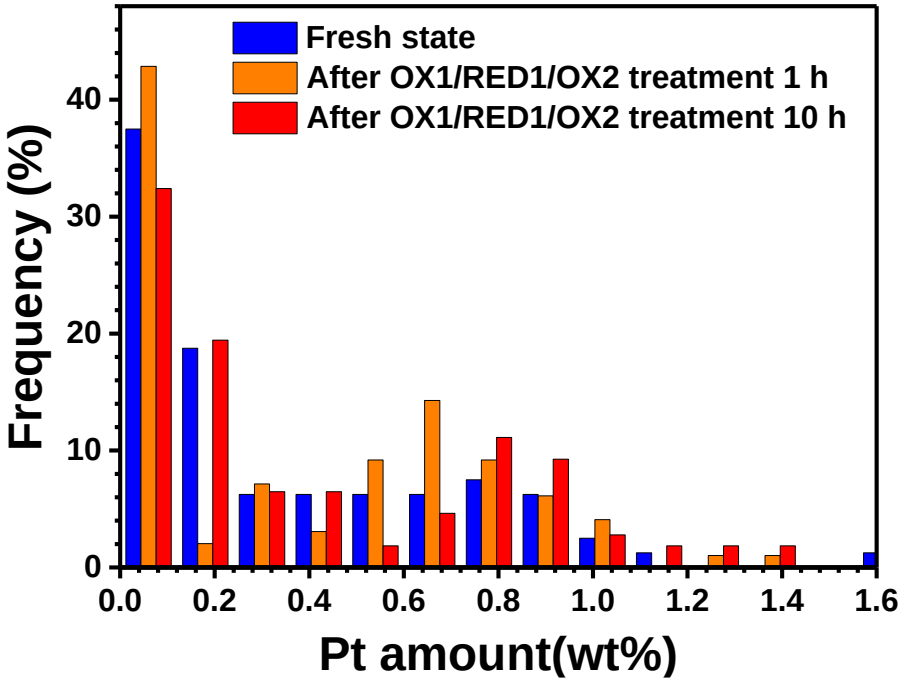

Figure 3. Distribution of Pt amount (wt%) determined by EDX analysis in a 0.80Pt+CeO_2 (1/1) mechanical mixture in the fresh state, after OX1, RED1 and OX2 treatments applied consecutively for 1 h each, and after OX1, RED1 and OX2 treatments applied consecutively for 10 h each.

Figure S4 compares the averaged Raman spectra of the whole analysed area (400 × 400 µm) in the fresh state and after successive redox treatments. The same bands as for the pure 0.80Pt sample were observed in the fresh state, with however a lower relative intensity of the PtO_x bands due to a lower Pt amount (one half) in the mixture. The band at 1050 cm^{-1} reveals the presence of carbonates (vibration $\nu 1$ of $(CO_3)^{2-}$ anion)[42] on the surface of bare CeO_2. The bands located at 2885 and at 2936-2978 cm^{-1} were attributed to formate species (ν(C-H) and δ(C-H)+ν_{as}(OCO) vibrations, respectively).[43,44] The disappearance of these species after OX1 shows that they are decomposed during this treatment. Upon the redox treatments, the same spectral evolution as that of the 0.80Pt sample is observed, with appearance of the electronic Raman band of Ce^{3+} at 2130 cm^{-1} after reduction and lower and higher relative intensities for the $\nu(PtO_x)$ and ν(O=O) bands, respectively, after reoxidation.

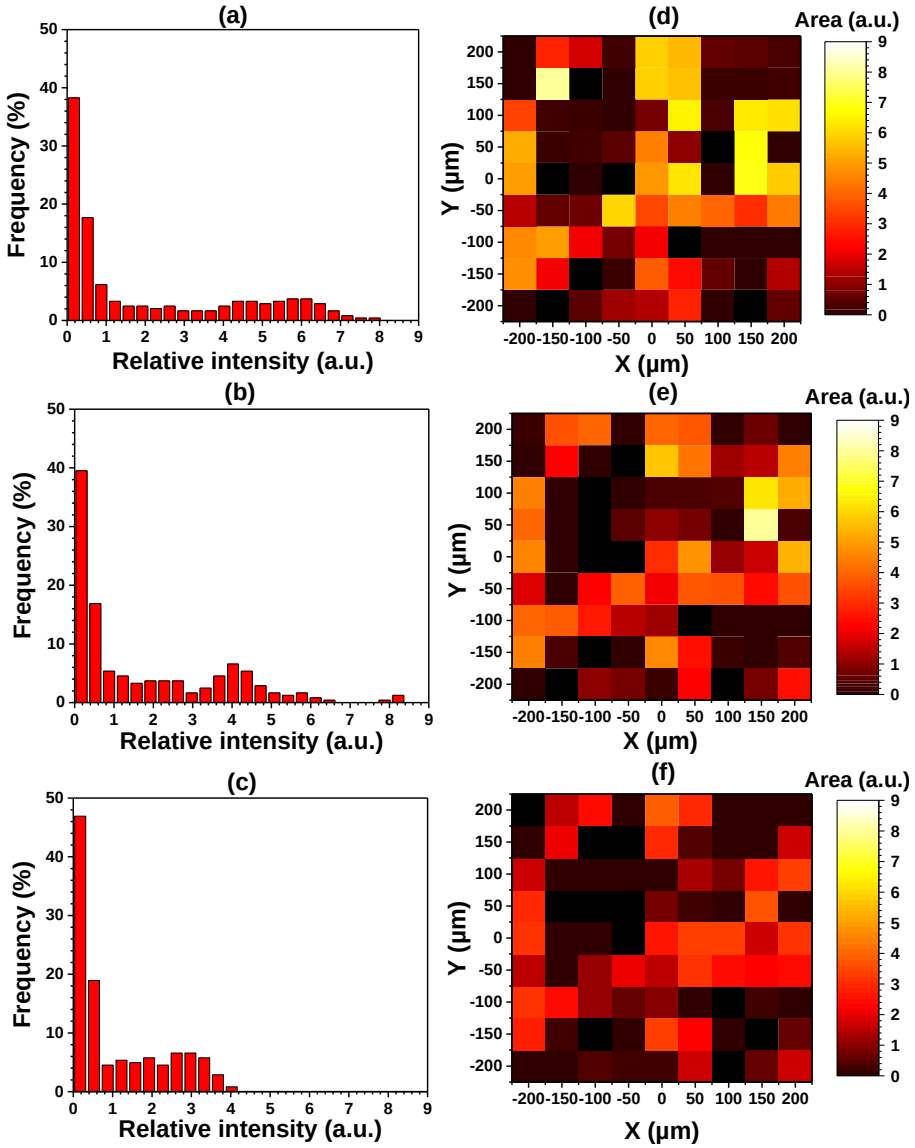

Figure 4. Distribution and Raman hyperspectral image of the relative intensity of the PtO_x band at 650 cm^{-1} for a 0.80Pt+CeO_2 (1/1) mechanical mixture in the a,d) fresh state and after b, e) OX1 and c, f) OX2 treatments. The area was determined between 650 and 750 cm^{-1} after baseline subtraction and normalization to the amplitude of the F_{2g} band.

A first statistical analysis of the areas of the PtO_x band at 650 cm^{-1} was carried out in the fresh state (Figure 4a): the presence of the two populations shows that the analysis method is suitable for observing the heterogeneity of the mechanical mixture at the micrometric scale. After the OX1 and OX2 treatments, the histograms still show two distinct populations (Figures 4b and 4c, respectively).

The histograms of the relative intensity of the ν(O=O) band and the corresponding fittings with two gaussian functions are plotted in Figures 5a-c. In case of platinum diffusion, the centres of the two functions should converge during the treatments. Instead, the center position of the first Gaussian remains constant and close to zero, whereas the second one is significantly shifted. An opposite trend is observed for the relative intensity of the PtO_x band (Figure 4a-c) although the histograms could not be fitted with two gaussian functions. It suggests that a change of the redox properties of the mechanical mixture occurred during the treatments.

In the fresh state, the hyperspectral Raman images of the relative intensity of the PtO_x and peroxo bands (Figures 4d and 5d, respectively) show light-yellow pixels corresponding to areas where the amounts of PtO_x and peroxo species are high. On the contrary, the dark pixels correspond to areas where they are essentially absent.

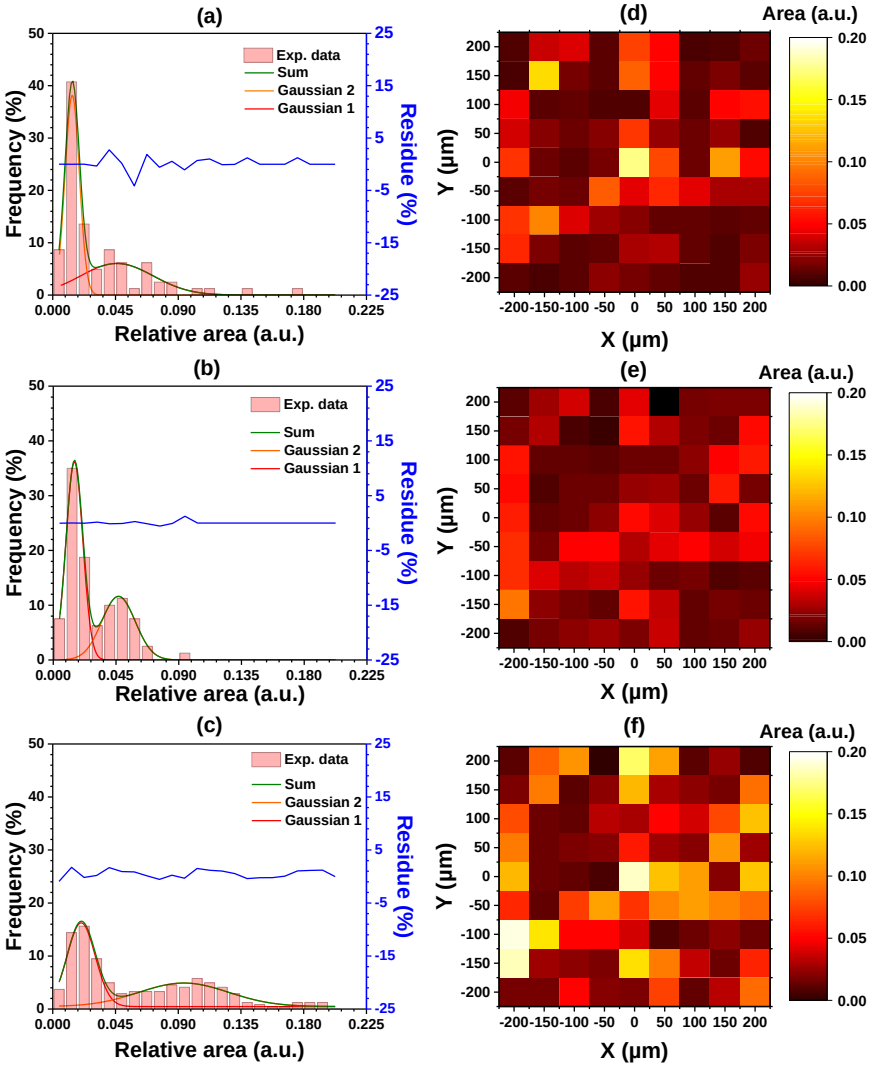

Figure 5. Experimental and fitted distribution, and Raman hyperspectral image of the relative intensity of ν(O=O) band for 0.80Pt+CeO_2 (1/1) mechanical mixture in the (a,d) fresh state and after (b,e) OX1 and (c,f) OX2 treatments. The area was determined between 750 and 900 cm^{-1} after baseline subtraction and normalization to the amplitude of the F_{2g} band.

The positive and high value (0.80 for a maximal value of 1, Table S1) of the correlation coefficient between the two matrices evidences a spatial correlation between the amounts of platinum and peroxo species on the surface, confirming that the presence of Pt^{2+} cations generates oxygen vacancies and stabilizes peroxo species. The relative deviations from the mean values at the different oxidized states (Table S2) and the correlation coefficients of the PtO_x band (Table S3) between fresh and OX1 states, and between OX1 and OX2 states, are still high (>0.95 and >0.75, respectively), which shows that platinum atoms remained located in the same agglomerates as in the fresh state, and that no homogenization occurred after thermal treatment under O_2 at 500 °C and a redox cycle at 500 °C. However, considering the spatial resolution of Raman spectroscopy, one cannot rule out Pt redistribution at nanoscale level around contacts between agglomerates.

Furthermore, the spatial correlation between PtO_x and peroxo species after the OX1 and OX2 treatments is confirmed (correlation coefficients of 0.81 and 0.92, respectively, Table S1).

Two populations can also be distinguished for the relative intensity of the Ce^{3+} electronic Raman band after RED1 and RED2 treatments (Figures 6a and 6b, respectively). The first one between 0 and 0.08 corresponds to the platinum-free ceria agglomerates. Indeed, bare CeO_2 is poorly reduced under H_2 at 500 °C[45] with possible formation of Ce^{4+}-H^- pairs,[46] which explains the absence of the Ce^{3+} band in the Raman spectrum (Figures S5 and 6e), unlike for 0.80Pt (Figures 1 and 6f). The high values (especially for the second cycle: 0.81, Table S1) of the correlation coefficient between the PtO_x and Ce^{3+} bands support this conclusion. Hence, the dark pixels in Figures 6c and 6d correspond to agglomerates of bare CeO_2. The frequency of these intensities is quite close to 50% (Figure 6a and b), confirming that platinum atoms do not diffuse between the ceria agglomerates at 500 °C under H_2. Note that deposition of only 0.1 wt% of Pt on CeO_2 is enough to significantly reduce the ceria surface to similar extent as with 0.80Pt below 500 °C (H_2 consumption degrees derived from TPR curves plotted in Figure S6 of 357 and 477 μmol.g^{-1}, respectively).

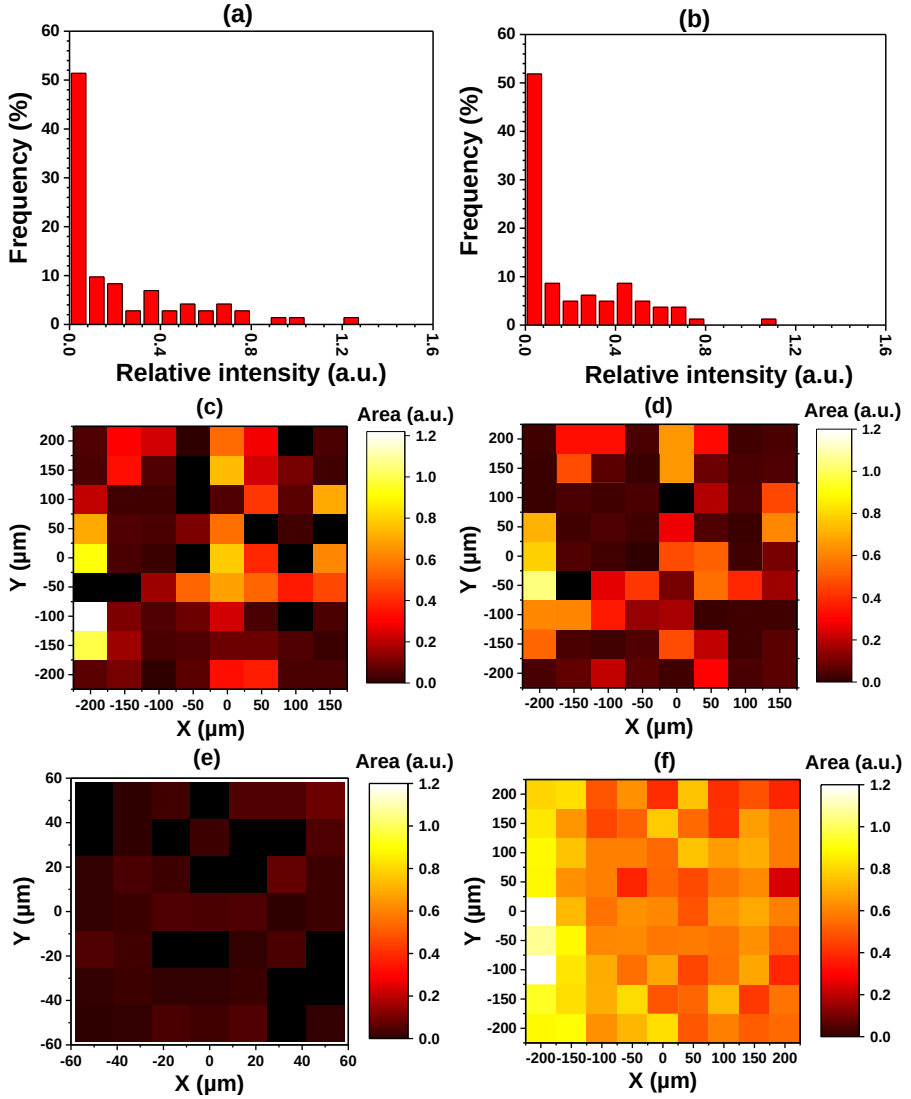

Figure 6. Distribution and Raman hyperspectral image of the relative intensity of the Ce^{3+} electronic Raman band for a 0.80Pt+CeO_2 (1/1) mechanical mixture after (a,c) RED1 treatment and after (b, d) RED2, and Raman hyperspectral image of the relative intensity of the Ce^{3+} electronic Raman band for

(e) CeO_2 and (f) 0.80Pt after RED1 treatment. The area was determined between 2050 and 2200 cm^{-1} after baseline subtraction and normalization to the amplitude of the 2LO band.

Surprisingly, the 0.80Pt+CeO_2 (1/1) mechanical mixture shows adsorbed peroxo species after both RED1 and RED2 treatments (Figure 7a and b, respectively) contrarily to the 0.80Pt sample alone (Figures 1 and 7d). These species may arise from chemisorption of residual O_2 at the surface of oxygen vacancies, inducing the oxidation of two Ce^{3+} cations to Ce^{4+} ones for each peroxo species formed (Scheme S1).[47] They were not observed after reduction of 0.80Pt probably because of further reoxidation at RT toward formation of O^{2-} anions.[48] In contrast, this band was observed for reduced bare ceria while the Ce^{3+} band was not detected (Figure S5). Hence, regions with high intensity in the hyperspectral images of the mechanical mixture after RED1 correspond to agglomerates of bare CeO_2 and those with low intensity to agglomerates of 0.80Pt. The high and negative values (-0.65 and -0.50, Table S1) of the correlation coefficient between the Ce^{3+} and the peroxo bands at the reduced states support this conclusion.

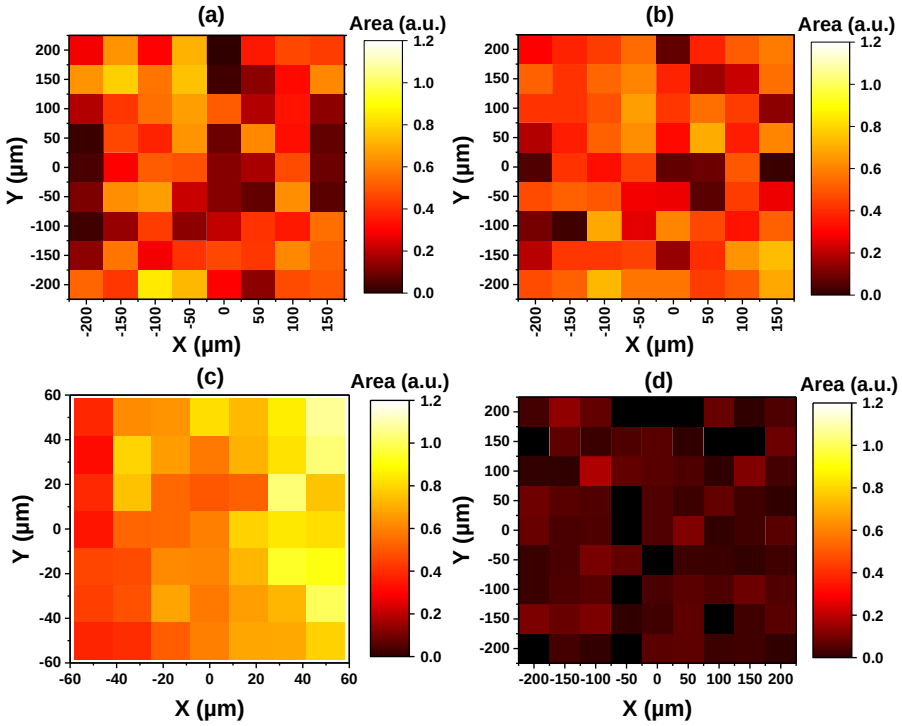

Figure 7. Raman hyperspectral images of the intensity of the ν(O=O) band of a 0.80Pt+CeO_2 (1/1) mechanical mixture after (a) RED1 and (b) RED2 treatment, after RED1 of (c) CeO_2 et (d) of 0.8Pt. The area was determined between 750 and 900 cm^{-1} after baseline subtraction and normalization to the amplitude of the F_{2g} band.

Conclusion

In this work, an original method was used to evaluate the dynamics of Pt/CeO_2 catalysts at the powder agglomerate scale during redox cycles at 500 °C. It combines SEM-EDX analyses and in situ optical and microRaman hyperspectral images performed on a Pt/CeO_2+CeO_2 mechanical mixture. All those techniques point to an absence of surface diffusion of platinum from one agglomerate to another. Notably, hyperspectral images of the Ce^{3+} electronic Raman bands and the ν(O=O) bands, which are highly sensitive to the presence of Pt at the reduced state, strengthen this conclusion. This work indicates that Pt surface diffusion takes place only at the nanometer scale and could be limited by atom trapping on Pt/CeO_2 agglomerates since numerous sites are potentially available. Therefore,

regeneration of aged catalysts, for which Pt is heterogeneously distributed at the agglomerate scale, would require a thermal treatment at higher temperature using the PtO_2 vaporization/trapping process. We suggest that the kinetics and the thermodynamics of this process could be studied by the novel methodology proposed in this manuscript.

Experimental Section

Materials

Tetraamineplatinum(II) nitrate $Pt(NH_3)_4(NO_3)_2$ precursor was purchased from Sigma-Aldrich (>99% purity). High surface area (150 $m^2.g^{-1}$) CeO_2 was provided by Solvay Special Chem Company.

Preparation

A Pt/CeO_2 sample was prepared by wet impregnation of 2 g CeO_2 with 24 mL of deionized water containing 38 mg of $[Pt(NH_3)_4](NO_3)_2$ (1.0 theoretical wt% Pt) at 60 °C for 4 h under stirring at 400 rpm. Water was then removed with a rotary evaporator at a temperature of 70 °C and a pressure of 200 mbar. The obtained powder was finally calcinated under 100 $mL.min^{-1}$ of synthetic air at 500 °C for 4 h with a heating rate of 10 $°C.min^{-1}$.

Different mechanical mixtures of this solid with pure CeO_2 were prepared by sieving the powder agglomerates between 50 and 80 µm before mixing them in different proportions. As shown by SEM image (Fig. S7), each agglomerate was composed of very small primary particles corresponding to one or very few crystallites.

Characterization tools

X-Ray Diffraction (XRD)

The samples were crushed and sieved below 50 µm before XRD analyses to avoid preferential orientations. Poly(methyl methacrylate) supports were used to analyse the powders with a D8 Advance 25 (Bruker) diffractometer equipped with a LynxEye XE-T detector. The X-Ray source was composed of a tungsten cathode and a copper anode. The Kα ray of Cu (λ=1.54184 Å) was selected with a Ni filter. The diffractogram was collected in the angular range from 4 to 80 ° with a step of 0.02 ° with a counting time of 0.5 s per step. The background and the Kα2 signal were removed using the DIFFRAC.EVA software.

Inductively Coupled Plasma-Optical Emission Spectrometry (ICP-OES)

The Pt/CeO_2 sample was dissolved into H_2SO_4+HNO_3+HCl mixture heated at 200 °C. The solution was diluted before being injected into an ACTIVA ICP-OES spectrometer (Jobin Yvon). Platinum elemental analysis was performed from the bands at 265.945 and 214.423 nm.

Annular Dark-Feld Scanning Transmission Electron Microscopy (ADF-STEM)

A Titan ETEM G2 80-300 kV (FEI) microscope equipped with a spherical aberration corrector was operated at 300 kV for the analyses, which were mainly carried out in ADF-STEM mode with a resolution of 0.136 nm. For each preparation, a few milligrams of the sample were ground and ultrasonically suspended in ethanol. Two to three drops of the suspension were deposited on the surface of the holey carbon film covering a 300 mesh copper grid.

Nitrogen adsorption volumetry

The specific surface area of the samples (150 mg) was determined by nitrogen physisorption volumetry at -196 °C with an ASAP 2020 (Micromeritics) apparatus after pretreatment at 300 °C under vacuum (10^{-3} mbar) using a Smart VacPrep (Micromeritics) device. The area was calculated from the Brunauer, Emmett and Teller (BET) equation.

SEM-EDX

Samples were compressed under 1 ton in the form of pellets before any analysis. Scanning electron microscopy (SEM) combined with energy dispersive X-ray spectroscopy (EDX) was carried out on a QUATTRO ESEM (ThermoFischer Scientific, EDX detector from Oxford Instruments) apparatus after redox treatments which consisted of oxidation under 20%O_2-N_2 at 500 °C (OX1), reduction under 20%H_2-N_2 at 500 °C (RED1) and reoxidation (OX2) under the same conditions as for OX1. The duration of each treatment was 1 or 10 h, the flow rate was 120 mL.min^{-1}, and the heating rate was 10 °C.min^{-1}. The SEM images were recorded ex situ at a voltage of 20 kV and a magnification of 2500. The EDX analysis of the sample was carried out statistically (100 analysed areas) before and after redox treatments with a spot size of 2 × 2 µm by counting for 40 s per spot. The M band at 2.1 eV was used for quantification with the Aztec software.

In situ Raman microspectroscopy

Raman spectra were recorded with a LabRAM HR (Horiba) spectrometer equipped with an Open Electrode CCD detector cooled at -75 °C. The Ar ion laser at 514 nm (power limited to 0.3 mW) was focused with an x50 objective, leading to a spatial resolution of ca. 2 µm. The backscattered light was recollected, sent to an Edge filter to remove the Rayleigh light, and spatially dispersed using a 300 lines.mm^{-1} diffraction grating, leading to a spectral resolution of 4 cm^{-1}. The acquisition time was 40 s for the 100-700 cm^{-1} spectral range and 450 s for the 700-4000 cm^{-1} one.

Mappings of 400 × 400 µm areas were carried out with a step of 50 µm, leading to a matrix of 81 Raman spectra. The sample was treated in a THMS600 (Linkam) cell at 500 °C for 1 h under 40 mL.min^{-1} synthetic air to remove surface species (OX1). It was then reduced under 40 mL.min^{-1} of 20% H_2-N_2 for 1 h (RED1). A second redox cycle was finally achieved in identical conditions (treatments labelled OX2 and RED2). The spectra were recorded at room temperature after each treatment while keeping the same atmosphere. They were treated with the Labspec 5 software, which was also used to generate different Raman hyperspectral images from the spectral matrices.

H_2 temperature-programmed reduction

H_2-TPR curves were determined using a 9 Omnistar GSD 301 O2 (Pfeiffer Vacuum) mass spectrometer. 50 mg of sample was placed in a U shape reactor between two quartz fibber pads, pretreated under 40 mL.min^{-1} of synthetic air at 500 °C during 1 h, and then reduced under 40 mL.min^{-1} of 1% H_2-He by heating from 25 °C to 500 °C at a rate of 10 °C.min^{-1}. When the temperature reached 500 °C, the feed was switched to pure H_2 and kept for 1 h before cooling down.

Acknowledgements

Laurence Burel and Anne Bonhommé (IRC@Tech) are acknowledged for her technical supports during SEM-EDX and Raman experiments, respectively. The Lyon Doctoral School of Chemistry (ED206) is acknowledged for the scholarship of C. Molinet.

Keywords: Pt/CeO_2 • platinum diffusion • redox treatments • powder agglomerate scale

[1] A. I. Boronin, E. M. Slavinskaya, A. Figueroba, A. I. Stadnichenko, T. Yu. Kardash, O. A. Stonkus, E. A. Fedorova, V. V. Muravev, V. A. Svetlichnyi, A. Bruix, K. M. Neyman, Appl. Catal. B Environ. 2021, 286, 119931.

[2] Y. Li, M. Kottwitz, J. L. VincentM. J. Enright, Z. Liu, L. Zhang, J. Huang, S. D. Senanayake, W.-C. D. Yang, P. A. Crozier, R. G. Nuzzo, A. I. Frenkel, Nat. Commun. 2021, 12, 914.

[3] F. Morfin, T.-S. Nguyen, J.-L. Rousset, L. Piccolo, Appl. Catal. B: Environ. 2016, 197, 2–13.

[4] P. Li, X. Chen, Y. Li, J. W. Schwank, Catal. Today 2019, 327, 90–115.

[5] S. S. Naghavi, A. A. Emery, H. A. Hansen, F. Zhou, V. Ozolins, C. Wolverton, Nature Commun. 2017, 8, 285.

[6] A. M. Gänzler, M. Casapu, F. Maurer, H. Störmer, D. Gerthsen, G. Ferré, P. Vernoux, B. Bornmann, R. Frahm, V. Murzin, M. Nachtegaal, M. Votsmeier, J.-D. Grunwaldt, ACS Catal. 2018, 8, 4800–4811.

[7] W. Tan, S. Xie, D. Le, W. Diao, M. Wang, K.-B. Low, D. Austin, S. Hong, F. Gao, L. Dong, L. Ma, S. N. Ehrlich, T. S. Rahman, F. Liu, Nature Commun. 2022, 13, 7070.

[8] J. L. Vincent, P. A. Crozier, Nature Commun. 2021, 12, 5789.

[9] F. Maurer, J. Jelic, J. Wang, A. Gänzler, P. Dolcet, C. Wöll, Y. Wang, F. Studt, M. Casapu, J.-D. Grunwaldt, Nature Catal. 2020, 3, 824–833.

[10] A. Boubnov, S. Dahl, E. Johnson, A. P. Molina, S. B. Simonsen, F. M. Cano, S. Helveg, L. J. Lemus-Yegres, J.-D Grunwaldt, Appl. Catal. B Environ. 2012, 126, 315–325.

[11] A. M. Gänzler, M. Casapu, A. Boubnov, O. Müller, S. Conrad, H. Lichtenberg, R. Frahm, J. D. Grunwaldt, J. Catal. 2015, 328, 216–224.

[12] G. Ferré, M. Aouine, F. Bosselet, L. Burel, F. J. Cadete Santos Aires, C. Geantet, S. Ntais, F. Maurer, M. Casapu, J.-D. Grunwaldt, T. Epicier, S. Loridant, P. Vernoux, Catal. Sci. Technol. 2020, 10, 3904–3917.

[13] J. Dong, Y. Zhang, D. Li, A. Adogwa, S. Huang, M. Yang, J. Yang, Q. Jin, Appl. Catal. B: Environ. 2023, 330, 122662.

[14] Y. Nagai, T. Hirabayashi, K. Dohmae, N. Takagi, T. Minami, H. Shinjoh, S. Matsumoto, J. Catal. 2006, 242, 103–109.

[15] Y. Nagai, K. Dohmae, Y. Ikeda, N. Takagi, T. Tanabe, N. Hara, G. Guilera, S. Pascarelli, M. A. Newton, O. Kuno, H. Jiang, H. Shinjoh, S. Matsumoto, Angew. Chem. Int. Ed. 2008, 47, 9303–9306.

[16] Y. Nagai, RD Rev. Toyota CRDL 2011, 42, 43–50.

[17] J. Jones, H. Xiong, A. T. DeLaRiva, E. J. Peterson, H. Pham, S. R. Challa, G. Qi, S. Oh, M. H. Wiebenga, X. I. Pereira Hernández, Y. Wang, A. K. Datye, Science 2016, 353, 150–154.

[18] F. Dvorak, M. Farnesi Camellone, A. Tovt, N.-D. Tran, F. R. Negreiros, M. Vorokhta, T. Skala, I. Matolinova, J. Myslivecek, V. Matolıin, S. Fabris, Nature Commun. 2016, 7,10801.

[19] Y. Lykhach, A. Bruix, S. Fabris, V. Potin, I. Matolínová, V. Matolín, J. Libuda, K. M. Neyman, Catal. Sci. Technol. 2017, 7, 4315–4345.

[20] F. Maurer, J. Jelic, J. Wang, A. Gänzler, P. Dolcet, C. Wöll, Y. Wang, F. Studt, M. Casapu, J.-D. Grunwaldt, Nat. Catal. 2020, 3, 824–833.

[21] D. Kunwar, S. Zhou, A. DeLaRiva, E. J. Peterson, H. Xiong, X. I. Pereira-Hernández, S. C. Purdy, R. ter Veen, H. H. Brongersma, J. T. Miller, H. Hashiguchi, L. Kovarik, S. Lin, H. Guo, Y. Wang, A. K. Datye, ACS Catal. 2019, 9, 3978–3990.

[22] D. Kunwar, C. Carrillo, H. Xiong, E. Peterson, A. DeLaRiva, A. Ghosh, G. Qi, M. Yang, M. Wiebenga, S. Oh, W. Li, A. K. Datye, Appl. Catal. B: Environm. 2020, 266, 118598.

[23] H. Xiong, S. Lin, J. Goetze, P. Pletcher, H. Guo, L. Kovarik, K. Artyushkova, B. M. Weckhuysen, A. K. Datye, Angew. Chem. Int. Ed. 2017, 56, 8986–8991.

[24] K. Leistner, C. Gonzalez Braga, A.k Kumar, K. Kamasamudram, L. Olsson, Appl. Catal. B: Environm. 2019, 241, 338–350.

[25] N. W. Kwak, D.-K. Lim, S. J. Jeong, P. Byeon, S.-Y. Chung, W. Jung, Adv. Mater. Interfaces 2020, 7, 2000688.

[26] A. M. Gänzler, M. Casapu, P. Vernoux, S. Loridant, F. J. Cadete Santos Aires, T. Epicier, B. Betz, R. Hoyer, J.-D. Grunwaldt, Angew. Chem. Int. Ed. 2017, 56, 13078–13082.

[27] M. Farnesi Camellone, F. Dvořák, M. Vorokhta, A. Tovt, I. Khalakhan, V. Johánek, T. Skála, I. Matolínová, S. Fabris, J. Mysliveček, ACS Catal. 2022, 12, 4859–4871.

[28] Y. Zhou, C. Jin, Y. Li, W. Shen, Nano Today 2018, 20, 101–120.

[29] J. Wang, E. Sauter, A. Nefedov, S. Heißler, F. Maurer, M. Casapu, J.-D. Grunwaldt, Y. Wang, C. Wöll, J. Phys. Chem. C 2022, 126, 9051−9058.

[30] B. Sarma, J. Jelic, D. Neukum, D. E. Doronkin, X. Huang, F. Studt, J.-D. Grunwaldt, J. Phys. Chem. C 2023, 127, 3032−3046.

[31] L. Piccolo, Catal. Today 2021, 373, 80–97.

[32] T. Montini, M. Melchionna, M. Monai, P. Fornasiero, Chem. Rev. 2016, 116, 5987–6041.

[33] S. Loridant, Catal. Today 2021, 373, 98–111.

[34] M. S. Brogan, T. J. Dines, J. A. Cairns, J. Chem. Soc. Faraday Trans. 1994, 90, 1461–1466.

[35] W. Lin, A. A. Herzing, C. J. Kiely, I. E. Wachs, J. Phys. Chem. C 2008, 112, 5942–5951.

[36] D. Mukherjee, B.M. Reddy, Catal. Today 2018, 309, 227–235.

[37] F. Giordano, A. Trovarelli, C. de Leitenburg, M. Giona, J. Catal. 2000, 193, 273–282.

[38] A. M. El-Toni, S. Yin, Y. Hayasaka, T. Sato, J. Electroceramics 2006, 17, 9–14.

[39] D. Andreescu, G. Bulbul, R. Emrah Özel, A. Hayat, N. Sardesai, S. Andreescu, Environ. Sci. Nano 2014, 1, 445–458.

[40] I. N. Bazhukova, S. Yu. Sokovnin, V. G. Ilves, A. V. Myshkina, R. A. Vazirov, N. Pizurov, V. V. Kasyanov. Optical Materials 2019, 92, 136–142.

[41] L. Pastor-Pérez, E. V. Ramos-Fernández, A. Sepúlveda-Escribano, Int. J. Hydrog. Energy 2019, 44, 21837–21846.

[42] M. Swanson, V. V. Pushkarev, V. I. Kovalchuk, J. L. d'Itri, Catal. Lett. 2007, 116, 41–45.

[43] M. Ziemba, C. Hess. Catal. Sci. Technol. 2020, 10, 3720–3730.

[44] G. Busca, J. Lamotte, J.-C. Lavalley, V. Lorenzelli, J. Am. Chem. Soc. 1987, 109, 5197–5202.

[45] J. Kammert, J. Moon, Z. Wu, Chin. J. Catal. 2020, 41, 901–914.

[46] Z. Wu, Y. Cheng, F. Tao, L. Daemen, G. S. Foo, L. Nguyen, X. Zhang, A. Beste, A. J. Ramirez-Cuesta, J. Am. Chem. Soc. 2017, 139, 9721−9727.

[47] M. Daniel, S. Loridant, J. Raman Spectrosc. 2012, 43, 1312–1319.

[48] C. Li, Y. Song, Y. Chen, Q. Xin, X. Han, W. Li, Stud. Surf. Sci. Catal. 1997, 112, 439–446.

Entry for the Table of Contents

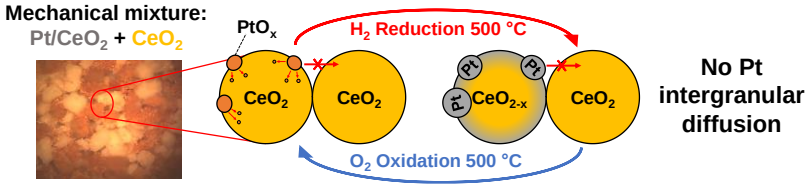

A methodology combining EDX analysis and in situ microRaman hyperspectral images has been performed on a mechanical mixture of Pt/CeO_2 and CeO_2 to follow Pt intergranular diffusion during redox treatments. Although platinum diffusion occurs on crystallite surface, intergranular Pt diffusion does not occur at 500 °C. It could be limited by atom trapping on Pt/CeO_2 agglomerates.

Twitter: @ircelyon